Evidence for abundant isolated magnetic nanoparticles at the Paleocene–Eocene boundary

Huapei Wang[a], Dennis V. Kent[a,b,1], and Michael J. Jackson[c]

[a]Earth and Planetary Sciences, Rutgers University, Piscataway, NJ 08854; [b]Lamont-Doherty Earth Observatory of Columbia University, Palisades, NY 10964; and [c]Institute for Rock Magnetism, Department of Geology and Geophysics, University of Minnesota, Minneapolis, MN 55455

Edited by Neil D. Opdyke, University of Florida, Gainesville, FL, and approved November 28, 2012 (received for review March 29, 2012)

New rock magnetic results (thermal fluctuation tomography, high-resolution first-order reversal curves and low temperature measurements) for samples from the Paleocene–Eocene thermal maximum and carbon isotope excursion in cored sections at Ancora and Wilson Lake on the Atlantic Coastal Plain of New Jersey indicate the presence of predominantly isolated, near-equidimensional single-domain magnetic particles rather than the chain patterns observed in a cultured magnetotactic bacteria sample or magnetofossils in extracts. The various published results can be reconciled with the recognition that chain magnetosomes tend to be preferentially extracted in the magnetic separation process but, as we show, may represent only a small fraction of the overall magnetic assemblage that accounts for the greatly enhanced magnetization of the carbon isotope excursion sediment but whose origin is thus unclear.

impact plume condensate | maghemite | magnetite | Ocean Drilling Program Leg 174AX

The Paleocene–Eocene boundary (~55.8 Ma) is marked by an abrupt negative carbon isotope excursion (CIE) (1, 2) that coincides with an oxygen isotope decrease interpreted as the Paleocene–Eocene thermal maximum (PETM) (3). In a cored section at Ancora (AN) (Ocean Drilling Program Leg 174AX) on the Atlantic Coastal Plain of New Jersey (Fig. 1), a zone of anomalously high magnetic susceptibility was discovered coincident with the CIE at the base of the Manasquan Formation (now known as the Marlboro Clay) (4). Bulk sediment magnetic hysteresis measurements indicated that the high magnetization corresponds to an increased abundance of very fine-grained magnetite with single domain (SD)-like magnetic properties. A similar association of high concentration of SD magnetite in a kaolinite-rich interval with minimum carbon isotope values was subsequently found in two other drill cores (Clayton and Bass River), which with the Ancora site, formed a transect across the New Jersey Atlantic Coastal Plain (5). The average distance between the magnetic particles is estimated to be 20 times larger than their lengths, given a concentration of 100 parts per million (ppm) estimated from the bulk saturation magnetization. Attempts to image the magnetic grains by transmission electron microscopy (TEM) in a bulk sample from the CIE interval in the Clayton site resulted in finding only a handful of isolated grains, which nevertheless had the requisite nanoscale dimensions (~50–70 nm) expected from the bulk hysteresis properties (5). Iron-rich nanophase material had been previously detected (with Mössbauer techniques) at several Cretaceous–Paleogene boundary sites and was ascribed to condensates from an impact ejecta plume (6, 7). Accordingly, the nanoparticle-rich interval associated with the CIE on the New Jersey Atlantic Coastal Plain was suggested to have a similar origin, providing circumstantial evidence for a major extraterrestrial (in this case cometary) impact at the onset of the CIE (5, 8).

Anomalously high concentrations of SD-like material have been confirmed by subsequent studies of the CIE from the Atlantic Coastal Plain, making these CIE sections perhaps the thickest dominated by SD magnetite recognized thus far in the stratigraphic record (9–13). In these studies, TEM observations on magnetic extracts were used to support the rock magnetic results and revealed the presence of chains of magnetic crystals that strongly resembled magnetofossils, with the implicit supposition that the separated fractions were representative of the entire magnetic assemblage. Unfortunately, most bulk magnetic properties such as hysteresis and first-order reversal curve (FORC) analyses are not able to establish if a SD-like grain assemblage is aligned in chains, the most distinctive crystallographic property for a biogenic origin (14). Some examples of naturally occurring SD-like assemblages in nature that are nonbiogenic include some pyroclastic tuffs (15), submarine basaltic glass (16), meteoritic smoke in polar ice cores (17), and even the magnetite nanoparticles of enigmatic origin in Martian meteorite ALH84001 (ref. 14; but see ref. 18).

In this paper, we present rock magnetic results from a relatively new technique, thermal fluctuation tomography (TFT) (19), as well as low temperature magnetic properties and high-resolution (HiRes) FORCs (20), in an effort to distinguish between isolated particles and chain structures. We selected for study the well-characterized Ancora (AN) core, making a comparison between sample AN560.1 from the CIE clay and sample AN567.7 from just before the CIE (Fig. 1); we also obtained supporting data from a CIE sediment sample from a shallower-water section cored at Wilson Lake (WL). Importantly, we compare magnetic results from a magnetic extract obtained from CIE bulk sample AN560.1 with those from a freeze-dried sample from an untreated culture of magnetotactic bacteria (MTB) MV-1 (21). These comparisons provide critical insights into the interpretation of the magnetic grain size and shape distribution in the CIE on which the origin of the magnetic particles is largely based and suggest a reevaluation of results from the more widely applied ferromagnetic resonance (FMR) technique (9, 12, 13).

Results

The magnetic particle size and shape distribution from TFT for Ancora CIE bulk sample AN560.1 (Fig. 2*A*) has a mode at length (L) = 56 nm and width-to-length aspect ratio (W/L) = 0.84. These TFT size and shape values are consistent with isolated near-equidimensional SD grains and TEM results on a bulk sample from the CIE (5). The TFT calculations for a sample from an untreated culture of MTB MV-1 (21) (Fig. 2*B*) show that the distribution of effective ferromagnetic particle sizes and shapes has multiple peaks that we interpret as corresponding to magnetosome chains (40 nm < L < 50 nm, 0.35 < W/L < 0.55) and individual particles (mode at L = 57 nm, W/L = 0.67), with a slightly larger major peak. These values are consistent with TEM images (12, 23, 24) but very different from the TFT results

Author contributions: H.W. and D.V.K. designed research; H.W. and M.J.J. performed research; M.J.J. contributed new reagents/analytic tools; H.W., D.V.K., and M.J.J. analyzed data; and H.W., D.V.K., and M.J.J. wrote the paper.

The authors declare no conflict of interest.

This article is a PNAS Direct Submission.

[1]To whom correspondence should be addressed. E-mail: dvk@rutgers.edu.

This article contains supporting information online at www.pnas.org/lookup/suppl/doi:10.1073/pnas.1205308110/-/DCSupplemental.

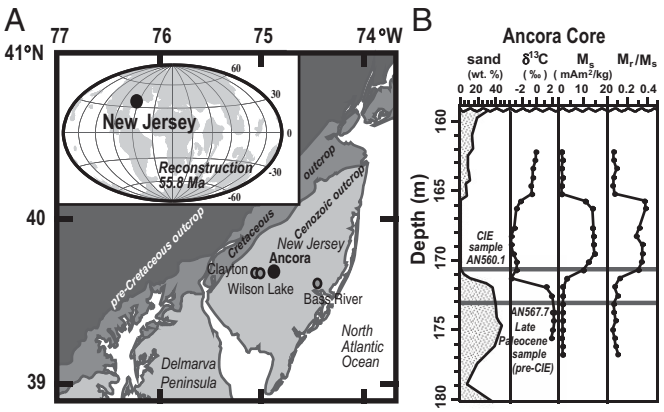

Fig. 1. (*A*) Location map for Ancora, Clayton, Wilson Lake, and Bass River drill sites on the Atlantic Coastal Plain of New Jersey. (*B*) Stratigraphic plots of sand percentage, bulk carbonate $\delta^{13}C$, saturation magnetization (Ms), and ratio of saturation remanence to saturation magnetization (Mr/Ms) for the interval in the Ancora cored section with the CIE (interval from ~171.5 m to ~165.5 m) with low $\delta^{13}C$ values (5). Positions are indicated of the CIE sample AN560.1 and the pre-CIE (Late Paleocene) sample AN567.7 from the Ancora core.

from the CIE bulk sample shown in Fig. 2*A*. This firstly reported TFT result for MV-1 shows the potential for detecting MTB magnetosome chains by the TFT technique.

The size and shape distribution for AN560.1 CIE magnetic extract residue (Fig. 2*C*) has a mode at L = 109 nm, W/L = 0.88, showing a much smaller tail toward the low W/L direction than the CIE bulk sample (Fig. 2*A*), indicating less elongated magnetic particles or fewer magnetosome chains. The TFT result for the AN560.1 CIE extract in its in situ state, derived by subtracting extract residue from bulk sediment data, shows two major peaks (Fig. 2*D*). One is around L = 100 nm, W/L = 0.9, very similar to the values for the extract residue (Fig. 2*C*); the other is around 40 < L < 50, 0.6 < W/L < 0.7, indicating more elongated particles or magnetosome chains.

The TFT size and shape distribution inferred for the CIE bulk sample more clearly impinges on the superparamagnetic (SP)–SD boundary than the MV-1 distribution, which is more tightly constrained within the SD field (Fig. 2 *A* and *B*). This might reflect a somewhat wider grain size distribution for the CIE clay than for the MV-1 magnetotactic bacteria sample, although the high M_r/M_s ratios preclude a large SP population in either case. The SP population can be imaged with low temperature TFT but requires cross-calibration to a different instrument than used for the high temperature TFT. A low temperature experiment was performed on a split of bulk sample AN560.1 but unfortunately the 300 K data in common did not match well (Fig. S1 *A* and *B*), indicating specimen differences or instrument offsets. However, 300 K data in common matched well (Fig. S1 *C* and *D*) for paired specimens of a bulk sample (WLb357.3) from an expanded section of the CIE from the B core at Wilson Lake, essentially the same as the

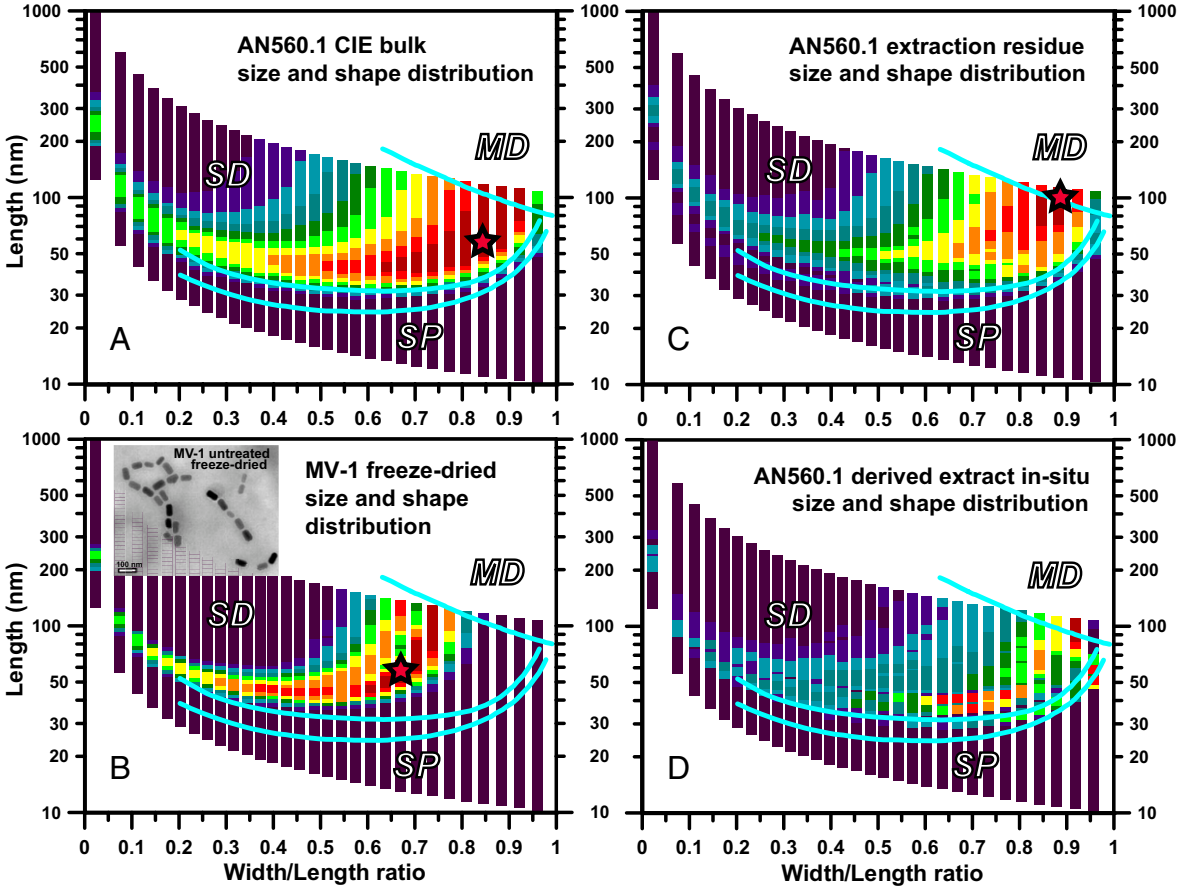

Fig. 2. TFT size and shape distributions calculated by back-field demagnetization (BFD) curves for (*A*) AN560.1 CIE bulk sediment, where a star marks the distribution mode. (*B*) Sample of laboratory cultured magnetotactic bacteria (MTB) MV-1 with TEM image of untreated freeze-dried MV-1 (12); a star marks the distribution mode that corresponds to individual magnetosome particles. (*C*) AN560.1 CIE magnetic extract residue, where a star marks the distribution mode. (*D*) AN560.1 CIE magnetic extract in its in situ state, derived by subtraction. Light blue lines delineate SP (superparamagnetic), SD (stable single domain), and MD (multidomain) regions in this parameter space (22). Color scale represents linear increments of probability density.

cored section investigated by others (9, 11, 25). The high temperature TFT results for WLb357.3 (Fig. S2*A*) are virtually identical to those of AN560.1 (Fig. 2*A*) with the TFT size and shape distribution patterns for CIE bulk sample WLb357.3 mainly showing a small shift in the SP direction along the trend of the SP–SD boundary line between the 300 K to 640 K range (mode at L = 65 nm, W/L = 0.84) and the 120 K to 640 K range (mode at L = 45 nm, W/L = 0.74) (Fig. S2 *A* and *B*).

Based on the field cooled and zero-field cooled (FC–ZFC) remanence warming curves (26) as well as low temperature demagnetization (LTD) cooling and warming curves of room temperature saturation isothermal remanence ($SIRM_{RT}$) from 5 K to 300 K), Verwey transitions (27) are observed at about 100–110 K for the CIE extract and at about 90–100 K for MV-1, with FC yielding higher remanence than ZFC, a typical signature for biogenic magnetosomes of SD magnetite (26) (Fig. 3 *A* and *B*). Although magnetic interactions may change the shape of FC–ZFC curves (28), a Verwey transition signal should still be present (29). The Verwey temperatures indicate that the magnetite particles in the CIE extract as well as the magnetosomes in the MV-1 culture are only partially oxidized. In contrast, the Verwey transition is not apparent for the CIE bulk samples (Fig. 3 *C* and *D*) and CIE magnetic extract residue (Fig. 3*E*), which we attribute to the dominant ferromagnetic mineral being SD maghemite (30) that formed either by crystallization in an oxidizing environment or by later oxidization of magnetite (31, 32). The presence of biogenic SD magnetite in the CIE extracts based on TEM observations (9–11) and our Verwey transition data for the CIE magnetic extract (Fig. 3*A*) suggest that the coexisting dominant SD maghemite particles and subordinate SD magnetite particles could be original independent components of the CIE sediments. A weak Verwey transition signal previously reported from a sample at the onset of the CIE from Wilson Lake (109.118 m depth) (11) may indicate a slightly higher biogenic SD magnetite portion. For the Ancora CIE bulk sample (Fig. 3 *C* and *D*), we also observe an inflection at around 37 K, which corresponds to the Neel temperature of siderite (33, 34). We estimate the mass concentration of siderite of about 1–2 ‰. In contrast, no clear trace of Verwey transition or siderite signal can be identified for the late Paleocene sample (AN567.7) just before the CIE (Fig. 3*F*).

A FORC diagram of AN560.1 CIE bulk (Fig. 4*A*) shows a narrow central ridge and faint reversible contributions appearing as a 45° asymmetric ridge, typical signatures for an assemblage of SD magnetic particles (20, 35). HiResFORC diagrams bring some characteristics into sharper focus and enable us to differentiate between the CIE bulk (Fig. 4*B*), CIE extract residue (Fig. 4*C*), CIE extract (Fig. 4*D*), and the extract in its in situ state derived by subtraction (Fig. 4*E*). From their coercivity profiles, it appears that there is a greater abundance of higher coercivity particles in the extract in its in situ state (Hc peaking at around 30–40 mT) than in the residue (Hc peaking at around 20–30 mT), indicating higher coercivity magnetosome chains are preferably extracted. A direct HiResFORC experiment on the AN560.1 CIE extract (Fig. 4*D*) shows a larger magnetic interaction signal, indicating that the extracted magnetic particles were probably crowded together around the magnet finger during extraction. A HiResFORC diagram for MTB MV-1 (Fig. 4*F*) also shows a narrow central ridge and clear reversible contribution. However, its coercivity profile is much more concentrated around 40 mT compared with the much broader coercivity profiles for the CIE bulk sample (Fig. 4*B*).

In light of the TFT data, we reanalyzed the reported FMR results for the laboratory cultured MTBs (12) and the CIE bulk samples (9) in a ΔB_{FWHM}-A plot (13) (Fig. 5). We find

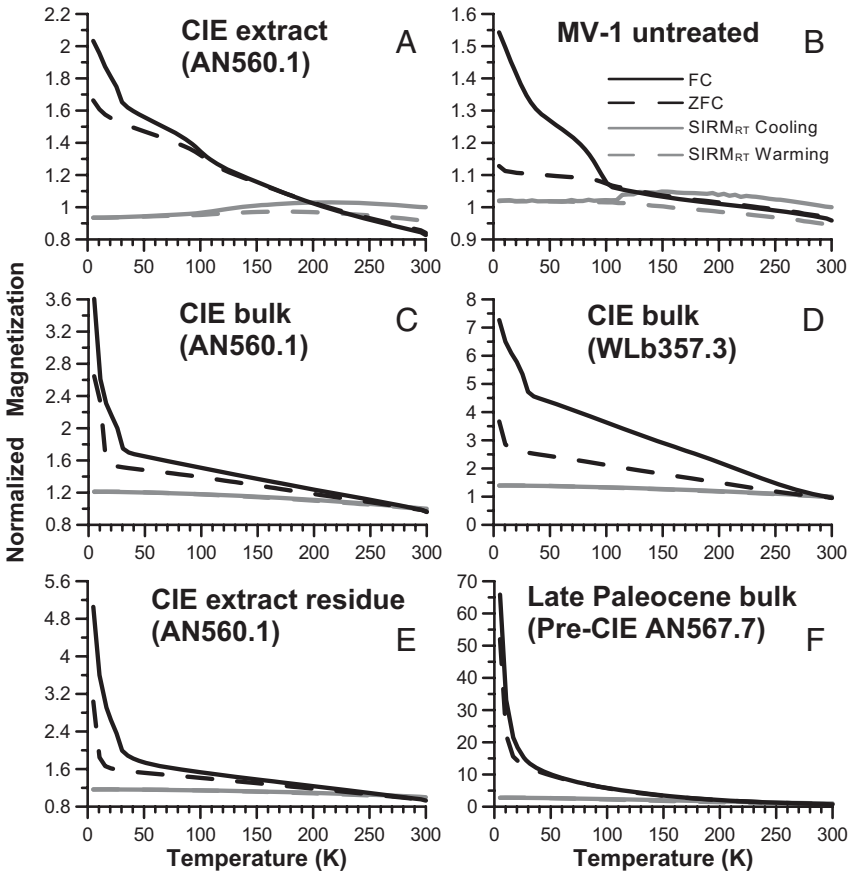

Fig. 3. Linearly normalized (to $SIRM_{RT}$) FC–ZFC and $SIRM_{RT}$ LTD curves for (*A*) AN560.1 CIE magnetic extract; (*B*) untreated freeze-dried cultured MTB sample of MV-1; (*C*) AN560.1 CIE bulk sediment; (*D*) WLb357.3 CIE bulk sediment; (*E*) AN560.1 CIE magnetic extract residue; and (*F*) AN567.7 late Paleocene (pre-CIE) bulk sediment.

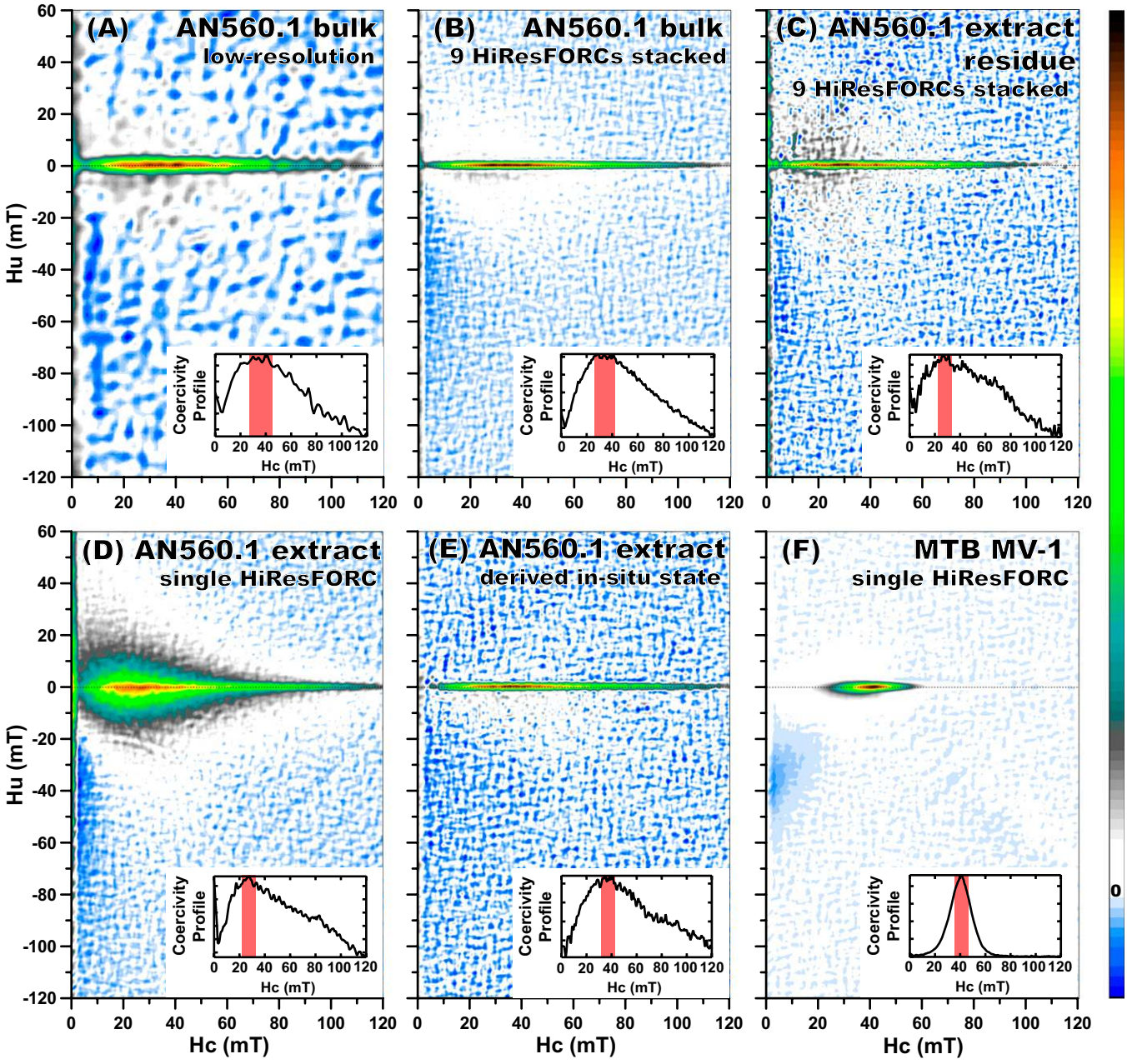

Fig. 4. FORC diagrams with inserts showing their coercivity (horizontal, Hu = 0) profiles, with peak coercivities marked by red bars. (*A*) AN560.1 CIE bulk sediment; (*B*) stacked (n = 9) HiResFORC for AN560.1 CIE bulk sediment; (*C*) stacked (n = 9) HiResFORC for magnetic extract residue; (*D*) single HiResFORC for AN560.1 CIE magnetic extract; (*E*) AN560.1 magnetic extract in its in situ state, derived by subtraction of (*C*) from (*B*); and (*F*) untreated freeze-dried cultured MTB sample of MV-1. All of the FORC diagrams share the same linear color scale on the right with 0 near the transition from white to light blue.

that the CIE bulk samples plot very close to sodium dodecyl sulfate (SDS)-treated and ultrasonicated *Magnetospirillum magneticum* strain AMB-1 mutant mnm18, which contains freed isolated approximately equidimensional magnetosome crystals. The reported FMR results of the CIE data compared with untreated and treated MTB data suggest a redefinition of the zones for lithogenic large grains, independent SD grains, and biogenic magnetosome chains in ΔB_{FWHM}-A parameter space (shaded ellipses in Fig. 5). In this perspective, the FMR data cannot exclude the interpretation that the ferromagnetic particles in the CIE clay are predominantly isolated near-equidimensional SD grains.

Discussion

We find that a broad array of rock magnetic results (TFT, FC–ZFC, LTD $SIRM_{RT}$, HiResFORC, and FMR) for CIE bulk samples from Ancora (and Wilson Lake) is consistent with the predominant presence of near-equidimensional noninteracting SD particles. These results allow alternative possibilities for the nature and origin of the dominantly SD magnetic particles that occur in greatly increased abundance in the CIE sediments. Populations of many different species of MTB, with differing magnetosome/chain geometries and admixed in suitable proportions, might conceivably produce similar TFT and FORC distributions. Such a hypothetical assemblage would indeed

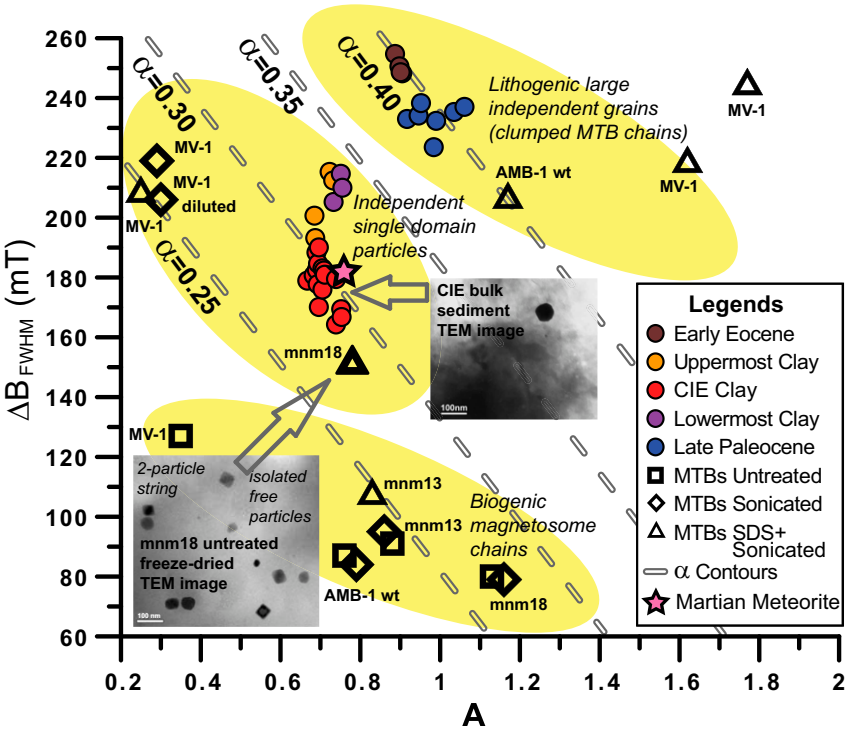

Fig. 5. FMR results of MTB data (12), CIE data (9), and Martian meteorite ALH84001 data (14) plotted in ΔB_{FWHM}-A parameter space (13). TEM images show the ferromagnetic particles of CIE clay (5) and untreated freeze-dried mnm18 (12) that consists of two-particle strings and isolated free particles (expected for SDS-treated and ultrasonicated sample). Zones of different magnetic origin are revised based on our assessment of all the plotted data.

provide a natural explanation for the sharp confinement of the size/shape distribution to the stable SD field, and for the relatively pure magnetite/maghemite composition, both resulting from biological control of magnetic particle formation. In contrast, the particle size distribution and mineralogical composition of impact plume condensates depend on many factors, and model calculations (36, 37) generally predict neither a narrow particle size distribution nor a preponderance of submicron sizes nor end member iron spinel compositions, and so these characteristics of the CIE sediments are rather fortuitous under the impact-plume scenario.

However, the TFT results show little indication of alignment in chains, a key signature of biogenic origin that also produces a distinct size and shape distribution in TFT results from cultured magnetotactic bacteria sample MV-1. The apparent discrepancy can be reconciled with the recognition that chain magnetosomes are preferentially extracted in the magnetic separation process (and subsequently imaged in TEM studies) but may be an unrepresentative small fraction of the overall magnetic assemblage in the CIE sediment. Fossil magnetosomes may very well become more prevalent during the CIE but the evidence is unclear whether they are solely or even mainly responsible for the greatly enhanced and geographically widespread SD-like magnetic properties of CIE bulk sediments. We would also point to the close resemblance of FMR parameters (Fig. 5) of CIE sediment and those reported for magnetic nanoparticles in Martian meteorite ALH84001, where it was concluded that no more than 10% of the magnetic particles were likely to be arranged in chains and thus difficult to prove to be of magnetosome origin (14). We believe our results are starting to build a similar case for the unusual SD-like characteristics of CIE sediment on the Atlantic Coastal Plain.

Materials and Methods

We performed a magnetic finger extraction procedure (9, 38) with a peristaltic pump circulation system at the Institute for Rock Magnetism (IRM) on CIE bulk sample AN560.1. The procedure was done using a very slow flow rate for over 24 h. Despite the deliberate care, we were able to extract only a small fraction of the total ferromagnetic particles as estimated by saturation remanent magnetization determined from hysteresis loops on the extract (5% of initial bulk value) and on the residue (94% of initial value), together indicating minimal (~1%) overall loss of the ferromagnetic minerals during the extraction procedure. TEM images on magnetic separates from Ancora CIE sediment reveal features like chain alignments that resemble bacterial magnetite (9), but at issue is how representative these observations are of the bulk of the CIE magnetic assemblage, which could just as well be largely composed of isolated equidimensional grains (5).

We conducted high temperature TFT (19) using a Princeton Measurements Corporation (PMC) vibrating sample magnetometer (VSM) equipped with a high temperature furnace (HT-VSM) at the IRM at the University of Minnesota on bulk samples from the CIE in the Ancora core to characterize the dominant W/L aspect ratio of the SD magnetic grains, which should approach 1 for isolated equidimensional grains and be much less than 1, depending on the effective elongations, for particles in chains. For bulk sample AN560.1 (170.72 m in the Ancora core, within the CIE; Fig. 1) and its magnetic extract residue, we measured back-field demagnetization (BFD) curves at logarithmic increments from 2 mT to 450 mT for 39 points from 300 K to 640 K (before any trace of severe chemical alteration sets in) at 10-K intervals. To avoid the undesirable effects of magnetostatic interactions introduced by the extraction process, we derived an unbiased estimate of the in situ BFD for the AN560.1 magnetic extract by subtracting each of the BFD curves of the extract residue from the BFD curves of the bulk sediment. We also conducted a TFT experiment on a sample from an untreated culture of MTB MV-1 (21), which was freeze dried and kept frozen for over 10 y (and thus likely to be partially oxidized), using backfield demagnetization curves from 300 K to 470 K at every 10 K for comparison (Fig. 2*B*).

We also conducted low temperature TFT (19) using another PMC VSM equipped with a low temperature cryostat (LT-VSM) at the IRM. We measured BFD curves at logarithmic increments from 2 mT to 1,500 mT for 45 points from 120 K (above the Verwey transition temperature) to 300 K at 10-K intervals. The BFD curves at 300 K on both instruments were almost identical after linear normalization for the specimens from the CIE bulk sample from Wilson Lake (WLb357.3; Fig. S1 *C* and *D*), allowing us to calculate the size–shape distribution using only high temperature data (Fig. S2*A*) and as well as by combining the high and low temperature data (Fig. S2*B*). Unfortunately, the 300-K BFD curves did not match the specimens from the CIE bulk sample from Ancora (AN560.1; Fig. S1 *A* and *B*), indicating specimen differences or instrumental offsets.

In the TFT calculations these temperature-dependent switching-field distributions are inverted to obtain the distribution of particle volumes and microcoercivities, f(V, H_k). For strongly magnetic cubic minerals such as magnetite and maghemite (we used Ms = 480 kA/m, which is appropriate

for magnetite although a somewhat lower value may apply for maghemite depending on exact composition), shape anisotropy dominates the magnetic behavior, and H_k is directly related to aspect ratio (22). The cells of the original rectangular (V, H_k) grid can thus be mapped into corresponding points in the (L, W/L) parameter space to represent the distribution of ferromagnetic particle lengths and aspect ratios, f(L, W/L) (Fig. 2*A*). The TFT inversion assumes that particles are noninteracting and that their moments reverse by coherent rotation. In intact chains of magnetosomes these assumptions are not satisfied, but we can anticipate the effects of this on the results. The critical field for incoherent reversal of magnetic moments in a chain of particles is somewhat larger than that for individual magnetosomes because interparticle interactions add to the anisotropy energy due to particle shape. Similarly the effective thermally activated volume is slightly larger than that of an individual magnetosome, due to the stabilizing effect of interactions along the chain. Thus, the expected behavior of intact chains in the TFT experiment is effectively that of isolated particles that are more elongate and slightly larger than individual magnetosomes, but much less elongate and smaller than the complete chains.

Low temperature magnetic properties were measured every 5 K for the CIE bulk samples (AN560.1 and WLb357.3), a late Paleocene (pre-CIE) bulk sample (AN567.7, 173.03 m in the Ancora core, Fig. 1), the CIE magnetic extract (AN560.1), the CIE extract residue, and the MV-1 culture, using the Quantum Designs magnetic properties measuring system (MPMS) at IRM (Fig. 3).

We performed regular FORC [field increment (δH) = 2 mT, smoothing factor (SF) = 3] and HiResFORC (δH = 0.6 mT, SF = 6) measurements (20) on the CIE bulk sample (AN560.1), the CIE extract, the CIE extraction residue, and MV-1, using a PMC alternating gradient force magnetometer (AGFM) at Rutgers University and analyzed the FORC data using FORCinel (39). For the CIE bulk sample and CIE extraction residue, we stacked nine HiResFORC measurements each by normalizing and averaging individual FORC measurements to improve the signal-to-noise ratio. We also performed subtraction of FORC results from CIE bulk and extraction residue to derive an unbiased FORC representation of the CIE extract in its in situ state.

ACKNOWLEDGMENTS. We thank Morgan F. Schaller and James D. Wright (Rutgers University) for discussions on the PETM/CIE that inspired this study, Bruce M. Moskowitz (Institute for Rock Magnetism, IRM) for the MV-1 sample, Robert E. Kopp (Rutgers University) for discussions on ferromagnetic resonance and magnetotactic bacteria, and two anonymous reviewers for constructive comments and suggestions. H.W. is grateful to the IRM for support of a Rock Magnetism Summer School and two Student Visiting Fellowships that allowed many of these measurements to be made and for support from a Schlanger Fellowship awarded by the National Science Foundation-sponsored US Science Support Program for the Integrated Ocean Drilling Program, which is administered by the Consortium for Ocean Leadership. This is contribution 7639 of Lamont-Doherty Earth Observatory.

1. Kennett JP, Stott LD (1991) Abrupt deep-sea warming, palaeoceanographic changes and benthic extinctions at the end of the Palaeocene. *Nature* 353:225–229.
2. Koch PL, Zachos JC, Gingerich PD (1992) Correlation between isotope records in marine and continental carbon reservoirs near the Paleocene Eocene boundary. *Nature* 358:319–322.
3. Zachos JC, Lohmann KC, Walker JCG, Wise SW (1993) Abrupt climate change and transient climates during the Paleogene: A marine perspective. *J Geol* 101:191–213.
4. Lanci L, Kent DV, Miller KG (2002) Detection of Late Cretaceous and Cenozoic sequence boundaries on the Atlantic coastal plain using core log integration of magnetic susceptibility and natural gamma ray measurements at Ancora, New Jersey. *J Geophys Res* 107:2216, 10.1029/2000JB000026.
5. Kent DV, et al. (2003) A case for a comet impact trigger for the Paleocene/Eocene thermal maximum and carbon isotope excursion. *Earth Planet Sci Lett* 211:13–26.
6. Verma HC, et al. (2001) Nano-sized iron phases at the K/T and P/T boundaries revealed by Mössbauer spectroscopy. *Lunar and Planetary Science XXXII* 1:1270.
7. Wdowiak TJ, et al. (2001) Presence of an iron-rich nanophase material in the upper layer of the Cretaceous-Tertiary boundary clay. *Meteorit Planet Sci* 36:123–133.
8. Cramer BS, Kent DV (2005) Bolide summer: The Paleocene/Eocene thermal maximum as a response to an extraterrestrial trigger. *Palaeogeogr Palaeoclimatol Palaeoecol* 224:144–166.
9. Kopp RE, et al. (2007) Magnetofossil spike during the Paleocene-Eocene thermal maximum: Ferromagnetic resonance, rock magnetic, and electron microscopy evidence from Ancora, New Jersey, United States. *Paleoceanography* 22:PA4103, 10.1029/2007PA001473.
10. Kopp RE, et al. (2009) An Appalachian Amazon? Magnetofossil evidence for the development of a tropical river-like system in the mid-Atlantic United States during the Paleocene-Eocene thermal maximum. *Paleoceanography* 24:PA4211, 10.1029/2009PA001783.
11. Lippert PC, Zachos JC (2007) A biogenic origin for anomalous fine-grained magnetic material at the Paleocene-Eocene boundary at Wilson Lake, New Jersey. *Paleoceanography* 22:PA4104, 10.1029/2007PA001471.
12. Kopp RE, et al. (2006) Ferromagnetic resonance spectroscopy for assessment of magnetic anisotropy and magnetostatic interactions: A case study of mutant magnetotactic bacteria. *J Geophys Res* 111:B12S25, 10.1029/2006JB004529.
13. Kopp RE, et al. (2006) Chains, clumps, and strings: Magnetofossil taphonomy with ferromagnetic resonance spectroscopy. *Earth Planet Sci Lett* 247:10–25.
14. Weiss BP, et al. (2004) Magnetic tests for magnetosome chains in Martian meteorite ALH84001. *Proc Natl Acad Sci USA* 101:8281–8284.
15. Schlinger CM, Veblen DR, Rosenbaum JG (1991) Magnetism and magnetic mineralogy of ash flow tuffs from Yucca Mountain, Nevada. *J Geophys Res* 96:6035–6052.
16. Pick T, Tauxe L (1993) Holocene paleointensities: Thellier experiments on submarine basaltic glass from the East Pacific Rise. *J Geophys Res* 98:17,949–17,964.
17. Lanci L, et al. (2012) Magnetization of polar ice: A measurement of terrestrial dust and extraterrestrial fallout. *Quat Sci Rev* 33:20–31.
18. Thomas-Keprta KL, Clemett SJ, Mckay DS, Gibson EK, Wentworth SJ (2009) Origins of magnetite nanocrystals in Martian meteorite ALH84001. *Geochim Cosmochim Acta* 73:6631–6677.
19. Jackson M, Carter-Stiglitz B, Egli R, Solheid P (2006) Characterizing the superparamagnetic grain distribution f(vi, H-k) by thermal fluctuation tomography. *J Geophys Res* 111:B12S07, 10.1029/2006JB004514.
20. Egli R, Chen AP, Winklhofer M, Kodama KP, Horng C-S (2010) Detection of noninteracting single domain particles using first-order reversal curve diagrams. *Geochem Geophys Geosyst* 11:Q01Z11, 10.1029/2009GC002916.
21. Dean AJ, Bazylinski DA (1999) Genome analysis of several marine, magnetotactic bacterial strains by pulsed-field gel electrophoresis. *Curr Microbiol* 39:219–225.
22. Butler RF, Banerjee SK (1975) Theoretical single-domain grain size range in magnetite and titanomagnetite. *J Geophys Res* 80:4049–4058.
23. Devouard B, et al. (1998) Magnetite from magnetotactic bacteria: Size distributions and twinning. *Am Mineral* 83:1387–1398.
24. Dunin-Borkowski RE, et al. (2001) Off-axis electron holography of magnetotactic bacteria: Magnetic microstructure of strains MV-1 and MS-1. *Eur J Mineral* 13: 671–684.
25. Zachos JC, et al. (2006) Extreme warming of mid-latitude coastal ocean during the Paleocene-Eocene Thermal Maximum: Inferences from TEX86 and isotope data. *Geology* 34:737–740.
26. Moskowitz BM, Frankel RB, Bazylinski DA (1993) Rock magnetic criteria for the detection of biogenic magnetite. *Earth Planet Sci Lett* 120:283–300.
27. Stacey FD, Banerjee SK (1974) *The Physical Principles of Rock Magnetism* (Elsevier, Amsterdam), 195 pp.
28. Carter-Stiglitz B, Jackson M, Moskowitz B (2002) Low-temperature remanence in stable single domain magnetite. *Geophys Res Lett* 29, 10.1029/2001gl014197.
29. Carter-Stiglitz B, Jackson M, Moskowitz B (2003) Correction to "low-temperature remanence in stable single domain magnetite" *Geophys Res Lett* 30, 10.1029/2003GL018727.
30. Ozdemir O, Dunlop DJ, Moskowitz BM (1993) The effect of oxidation on the Verwey transition in magnetite. *Geophys Res Lett* 20:1671–1674.
31. Colombo U, Fagherazzi G, Gazzarrini F, Lanzavecchia G, Sironi G (1968) Mechanism of low temperature oxidation of magnetites. *Nature* 219:1036–1037.
32. Gallagher KJ, Feitknecht W, Mannweiler U (1968) Mechanism of oxidation of magnetite to gamma-Fe2O3. *Nature* 217:1118–1121.
33. Frederichs T, von Dobeneck T, Bleil U, Dekkers MJ (2003) Towards the identification of siderite, rhodochrosite, and vivianite in sediments by their low-temperature magnetic properties. *Phys Chem Earth* 28:669–679.
34. Jacobs IS (1963) Metamagnetism of siderite (FeCO3). *J Appl Phys* 34:1106–1107.
35. Newell AJ (2005) A high-precision model of first-order reversal curve (FORC) functions for single-domain ferromagnets with uniaxial anisotropy. *Geochem Geophys Geosyst* 6:Q05010, 10.1029/2004GC000877.
36. Ebel DS, Grossman L (2005) Spinel-bearing spherules condensed from the Chicxulub impact-vapor plume. *Geology* 33:293–296.
37. Johnson B, Melosh H (2012) Formation of spherules in impact produced vapor plumes. *Icarus* 217:416–430.
38. Petersen N, Vondobeneck T, Vali H (1986) Fossil bacterial magnetite in deep-sea sediments from the South Atlantic Ocean. *Nature* 320:611–615.
39. Harrison RJ, Feinberg JM (2008) FORCinel: An improved algorithm for calculating first-order reversal curve distributions using locally weighted regression smoothing. *Geochem Geophys Geosyst* 9:Q05016, 10.1029/2008GC001987.

Supporting Information

Wang et al. 10.1073/pnas.1205308110

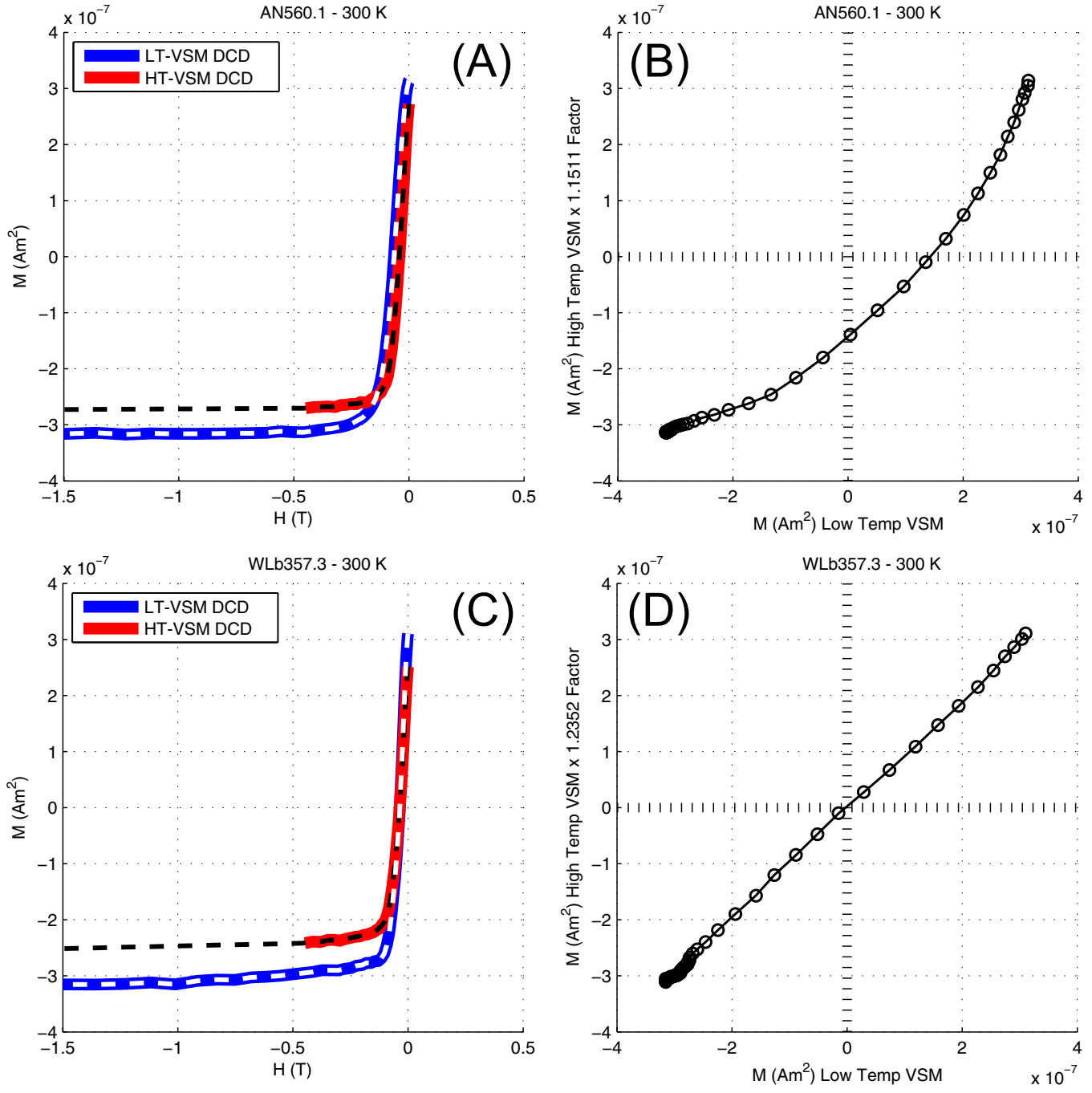

Fig. S1. Comparison of back-field demagnetization (BFD) curves at 300 K on high temperature (HT)-VSM (red) and low temperature (LT)-VSM (blue) for CIE bulk sediment samples AN560.1 (*A* and *B*) and WLb357.3 (*C* and *D*). BFD curve extrapolations (black dashed lines; *A* and *C*) were performed by the inverse of the 1.5-T saturation remanences. Comparisons of BFD remanences at 300 K measured with HT-VSM vs. LT-VSM for the same demagnetization steps are shown in *B* for AN560.1, which has poor agreement, and in *D* for WLb357.3, which has good agreement.

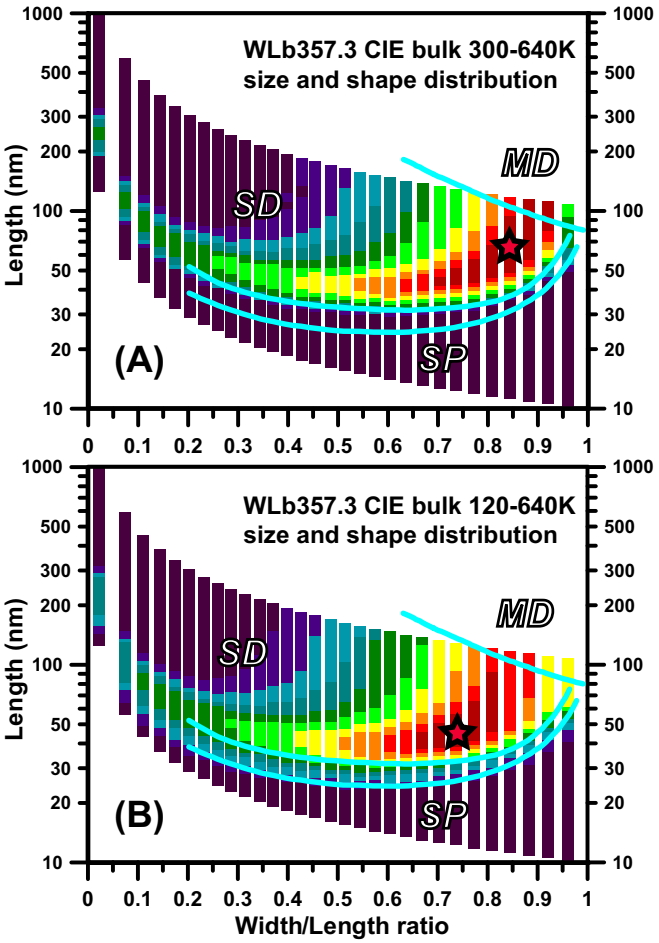

Fig. S2. Thermal fluctuation tomography (TFT) size and shape distributions for carbon isotope excursion (CIE) bulk sediment WLb357.3 calculated by back-field demagnetization (BFD) curves from (*A*) 300 K to 640 K and (*B*) 120 K to 640 K. Star, superparamagnetic (SP), single domain (SD), and multidomain (MD) as in Fig. 2.